We are IntechOpen, the world's leading publisher of Open Access books
Built by scientists, for scientists

6,900
Open access books available

186,000
International authors and editors

200M
Downloads

154
Countries delivered to

Our authors are among the

TOP 1%
most cited scientists

12.2%
Contributors from top 500 universities

CLARIVATE ANALYTICS
BOOK CITATION INDEX
INDEXED

WEB OF SCIENCE™

Selection of our books indexed in the Book Citation Index
in Web of Science™ Core Collection (BKCI)

Interested in publishing with us?
Contact book.department@intechopen.com

Numbers displayed above are based on latest data collected.
For more information visit www.intechopen.com

13

Microstructured Fibre Taper with Constant Outer Diameter

Ming-Leung Vincent Tse[1], D. Chen[1,2],
C. Lu[1], P. K. A. Wai[1] and H. Y. Tam[1]
[1]The Hong Kong Polytechnic University, Hong Kong SAR,
[2]Zhejiang Normal University,
China

1. Introduction

Microstructured Optical Fibres (MOFs) can be tapered in many ways depending on the length scale. Short taper of a few centimetres in length is commonly produced using the flame brush technique on a conventional fibre tapering rig (Bilodeau et al., 1988). Meso-taper of up to tens of metres in length can be produced using improved tapering rig with a ceramic microheater (Vukovic et al., 2008). It is also possible to taper optical fibre on a standard fibre draw tower, both for conventional step index fibre (Chernikov et al., 1993) and for MOFs (Tse et al., 2006b). Longitudinal variation of the MOF structure can lead to a comprehensive control of dispersion and nonlinearity, for spectral control under general conditions (Tse et al., 2008). The possibility of different long-length fibre-taper designs can lead to exciting applications in nonlinear fibre optics, such as uniform and stable supercontinuum generation for telecommunications spectral slicing (Chen et al., 2009a; Dudley & Coen, 2002; Genty et al., 2009; Vukovic & Broderick 2010), adiabatic soliton compression (Hu et al., 2006; Tse et al., 2006b, 2008), mode conversion (Town & Lizier, 2001) and pulse transformation (Broderick, 2010).

The early dispersion-decreasing microstructured fibres were fabricated by stacking of glass capillaries with radial (2D) designs consisted of uniform air hole size (Travers et al. 2007; Tse et al., 2006b). The preforms were drawn into canes (diameter in mm scale), and finally tapered down either by changing the pressure of all the air holes, or by reducing the outer diameter (OD) of the fibre during the drawing process. Both methods led to variation of hole and core sizes along the fibre. The disadvantage of such tapering schemes is that when the features reduce in size, the associated confinement loss increases (Marks et al. 2006; Nguyen et al., 2005). Therefore, a large number of rings of air holes are needed to reduce the loss to a low level; the fabrication of these MOFs is labour intensive. Moreover, decrease of the outer diameter of the fibre may reduce the mechanical strength of the fibre and handling may became difficulty, at the same time induce complication when connecting to standard fibres.

It has been reported that selective holes within the microstructure region of MOFs can be independently pressurised during the fibre drawing process (Couny et al. 2008). Together with the possibility to vary the pressure of the holes during the drawing process (Tse et al.,

2006b; Voyce et al. 2009), more complex 3D fibre designs can be achieved. A design concept is introduced for long microstructured fibre taper to be produced by stacking of silica capillaries, and to be drawn on a traditional optical fibre draw tower with multi-pressure control (Tse et al., 2009b).

In this chapter, we will investigate in detail the optical properties of these draw-tower tapers, in particular, the Effective Refractive Index (n_{eff}), Confinement Loss (CL), Dispersion (D) and Effective Mode Area (A_{eff}). In Section II, an outline of the concept of the proposed fibre tapering scheme and the simulation method will be presented. In Section III, the simulation result for the effective refractive index and confinement loss of the chosen fibre designs will be presented and discussed. Section IV investigates the dispersion profile and the effective mode area at different positions along various fibre tapers. In Section V, the proposed fabrication method and preliminary results will be presented. Final section summarises the results with conclusion.

2. Long microstructured fibre taper design concept

The proposed tapering scheme consists of microstructure features with large air-holes (high air-filling fraction) in every ring initially. The holes of the innermost rings are then tapered longitudinally by an independent pressure control, while keeping the outer diameter of the fibre constant by varying the draw speed at the same time. However, the variation of draw speed is not necessary for fibres with d << OD, because the variation of the glass volume is very small. Here, we investigate the simplest case, in which only the innermost ring-of-holes is varied in size. Thus, the core is made of 7-cell defects at the beginning of an index guiding taper, and the core is reduced to a 1-cell defect at the end of the taper, see Fig. 1. This tapering scheme offers low confinement loss over the entire length of the fibre, and large end-to-end core-size variation. Moreover, the mechanical strength of the fibre is the same throughout, because of the constant outer diameter. This concept has already found application in core expansion of MOFs using the flame brush method for fibre splicing, see (Chen et al., 2009b). However, the proposed draw-tower, multi-pressure MOF taper here should not be confused with tapers that are made on a tapering rig by post-processing methods after a fibre is drawn.

In this work, a full vector finite-element-method (FEM) based optical mode solver (Mode SolutionsTM 3.0 by Lumerical Solution Inc.) was used to study the fibre designs. Pure silica fibres are simulated. Dense grids consisting of large number of mesh cells (typically between 90,000 and 100,000), with emphasis at the centre region (where the guided modes were found), were used in the simulation to ensure accuracy. Perfectly matched layer (PML) boundary conditions were used. The effective index was also checked against a more commonly used simulation tool for modeling MOF (COMSOL Multiphysics), and similar results were found. The modal behaviour at different positions along various tapered MOFs for pump wavelength of 1060 nm was investigated. This wavelength coincides with that of efficient Yb-doped fibre laser sources. Dispersion profiles around 1060 nm were simulated.

MOFs with design consisting of 8 initial rings of air-holes are studied, with small hole-to-hole spacing (pitch), Λ, varied from 0.5 to 0.7 μm. The ultra-small pitch or core ensured the minimum effective mode area is obtained, and also reduced the multimodeness. The air-filling fraction, d_{2+}/Λ, of ring 2 to 8 varied from 0.6 to 0.9 for different fibres. The large
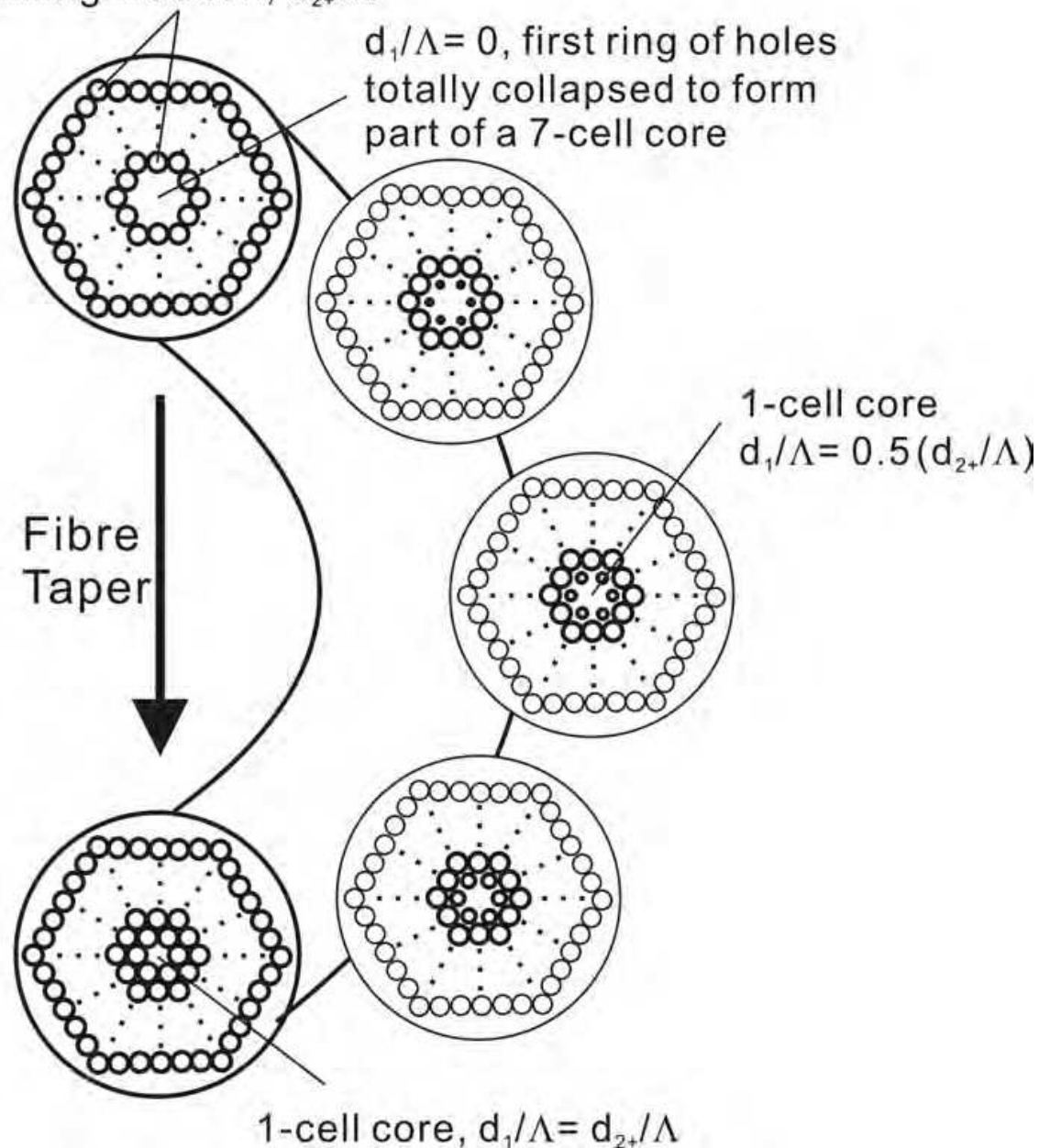
Fig. 1. A schematic of the proposed MOF taper scheme. Rings 2-8 consisted of large air-holes. The core-size is reduced by introducing the innermost ring of holes (ring 1). A 7-cell defect solid-core is found in the beginning of the fibre , which is formed partly by totally collapsing the holes in ring 1. A single-cell defect solid-core is found at the end of the fibre.

d_{2+}/Λ ensured low confinement loss. The air-filling fraction, d_1/Λ, of the innermost ring (ring 1) was varied from 0 to d_{2+}/Λ in each MOF taper. We studied the characteristics of each taper by simulating at least ten 2D cross-sections along the fibre. For example, when $d_{2+}/\Lambda = 0.9$, cross-sections with $d_1/\Lambda = 0, 0.1, 0.2…0.9$ were simulated.

3. Effective refractive index and confinement loss

In this section, we investigate the effective refractive index and confinement loss of long MOF tapers with different feature sizes. The simulated effective index of the fundamental mode and the first higher order mode along the fibres under investigation at 1060 nm are presented in Fig. 2. The result of the simulated associated confinement loss is presented in Fig. 3.

Fig. 2 shows that as the first ring-of-holes is being introduced (d_1/Λ increases), the effective index decreases, owing to the increased amount of mode field propagating in the air-holes. Therefore, as the core-size decreases (d_1/Λ increases), the confinement loss increases, see Fig. 3. It is more evident by looking at the mode field amplitude found from the simulated meshed structure. The mode field images of one of the taper design ($\Lambda = 0.6$ μm and $d_{2+}/\Lambda = 0.75$) are shown in Fig. 4. It shows that at the beginning of the taper with a 7-cell core ($d_1/\Lambda = 0$), the fundamental mode is well confined in the silica core. Near the middle of the taper ($d_1/\Lambda = 0.4$) and at the end of the taper ($d_1/\Lambda = 0.75$), significant amount of the mode field is propagating in the first ring of air-holes. For comparison, the mode fields of the 1st higher order mode are also shown in Fig. 4. The overlap of mode field and air is even more apparent for the higher order modes. The power in the air-holes will add an additional loss through scattering, as more power overlapping the air-glass boundary (White et al., 2002).

The confinement loss of the HE11 mode and higher order modes varied along the MOF tapers. We assumed for effectively single-mode guidance, the CL of the higher order mode is 10,000 times greater than that of the fundamental mode. Therefore, for each MOF taper design, part of the taper is effectively single-mode and part of the taper is slightly multi-mode. In general, the tapers are becoming more single-mode as d_1/Λ increases. The multi-mode to single-mode transition is indicated with an asterisk in Fig. 3. For $\Lambda = 0.6$ μm and $d_{2+}/\Lambda = 0.6$, the entire MOF taper is effectively single mode, however, loss is very high (up to 100 dB/m). We have also simulated the same MOF taper with fibre bending radius of 1 mm, and found that there is negligible changes to the loss. This is expected for all the structures consider here, as the cores are very small. Bending loss is usually more significant in Large Mode MOFs (Baggett et al., 2003).

Note that, the result is presented with a general fibre length scale. In practice, depending on how the pressure is varied with time during the drawing process, the length of particular portions of the fibre can be chosen according to application requirement. A MOF taper produced on a fibre draw tower can have length of a few metres up to kilometres.

4. Simulated dispersion profiles and effective mode areas

In this section, the dispersion profiles and the effective mode area at different position along the fibre tapers around 1060 nm are investigated. Dispersion profiles are studied in Section 4.1 and mode field areas are presented in Section 4.2.
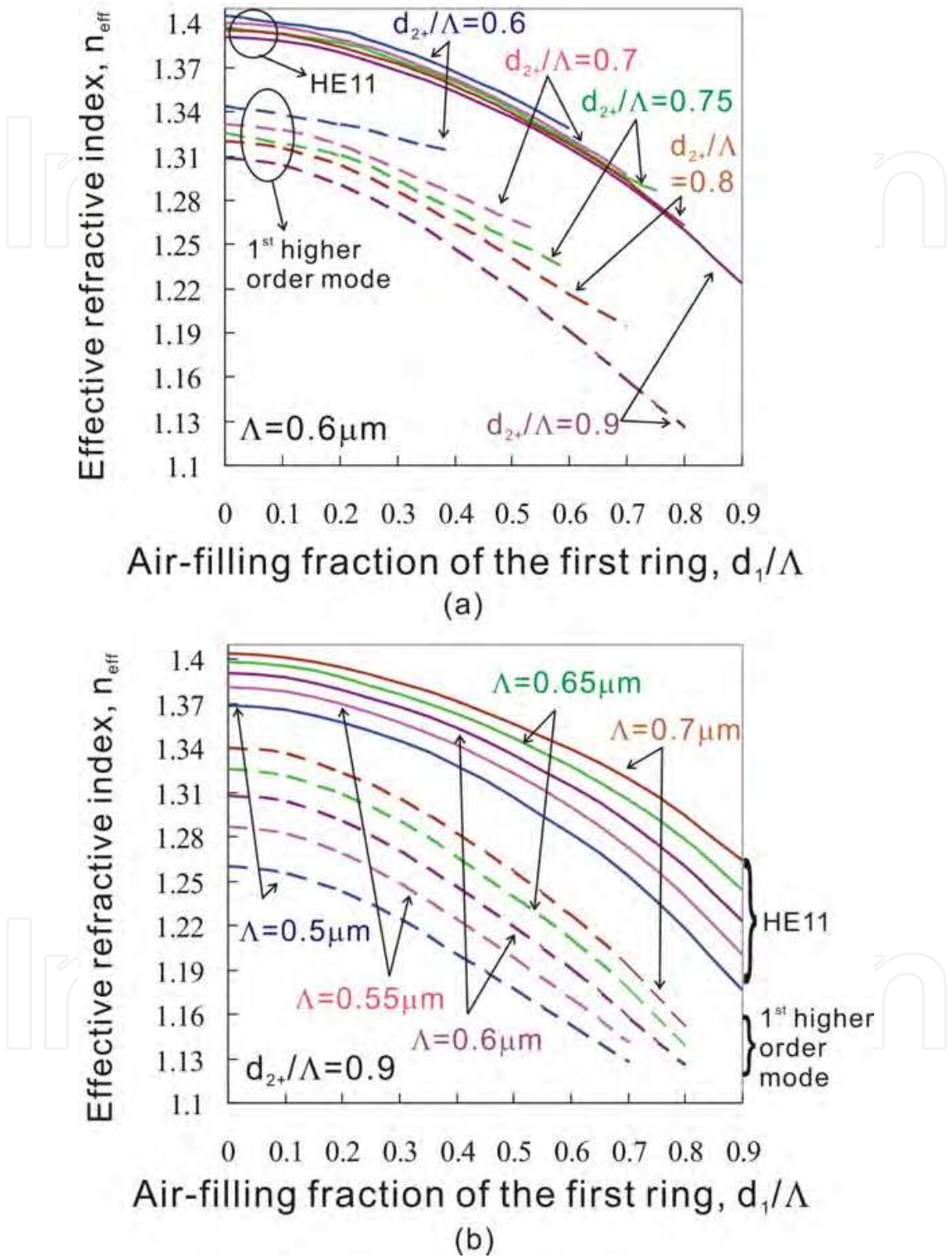
Fig. 2. Simulated effective refractive index of the HE11 mode (solid line) and the 1st higher order mode (dotted line) along tapers with different Λ and d_{2+}/Λ: (a) $\Lambda = 0.6$ μm, $d_{2+}/\Lambda = 0.6, 0.7, 0.75$ 0.8 and 0.9 (b) $d_{2+}/\Lambda = 0.9$, $\Lambda = 0.5, 0.55, 0.6, 0.65$ and 0.7 μm.
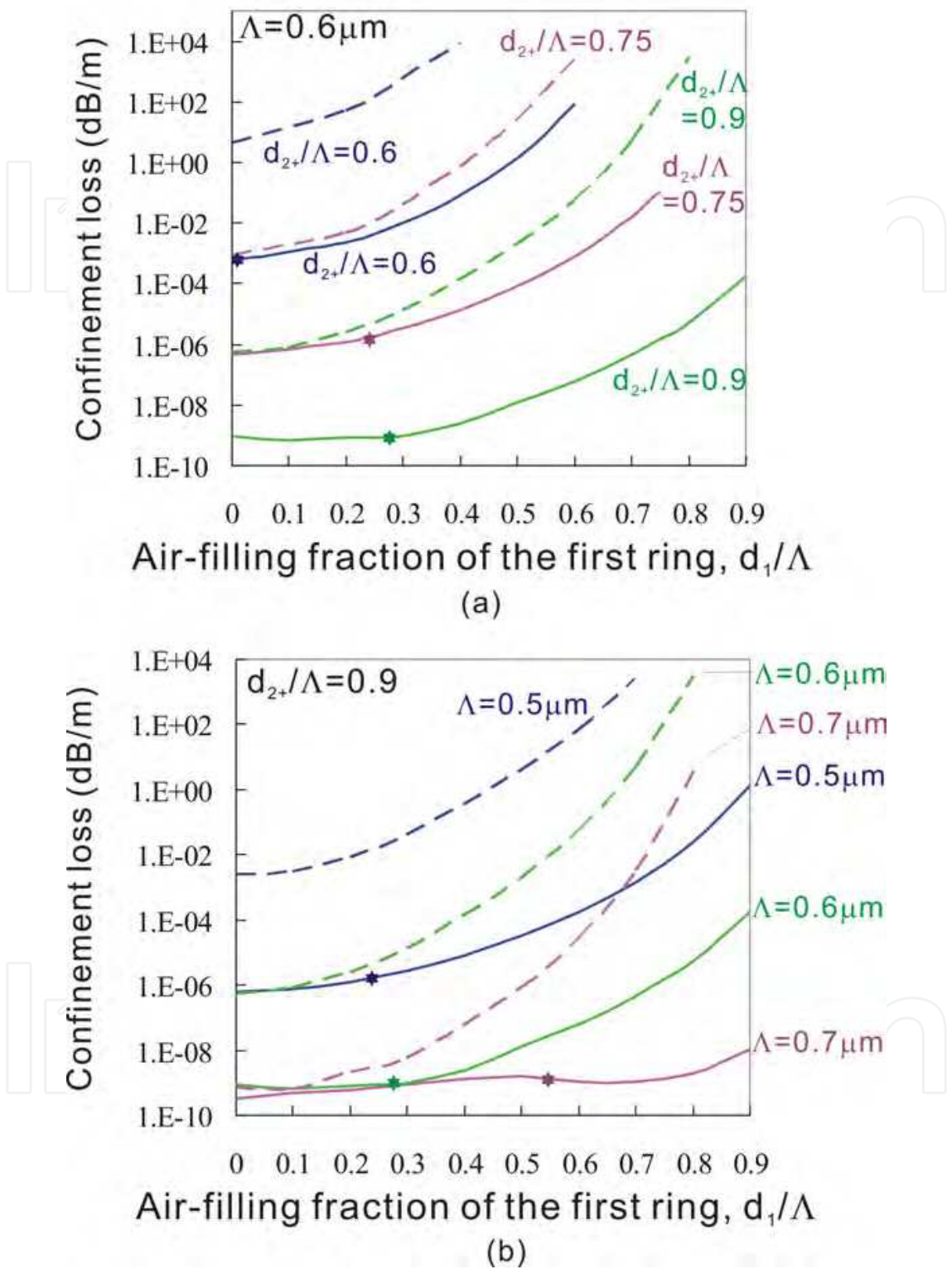
Fig. 3. Simulated confinement loss of the HE11 mode (solid line) and the 1st higher order mode (dotted line) along tapers with different Λ and d_{2+}/Λ: (a) Λ= 0.6 μm, d_{2+}/Λ= 0.6, 0.75 and 0.9 (b) d_{2+}/Λ= 0.9, Λ= 0.5, 0.6 and 0.7 μm. (Asterisks indicate where CL of the 1st higher order mode is 10,000 times larger than that of the fundamental mode)

$\Lambda=0.6$
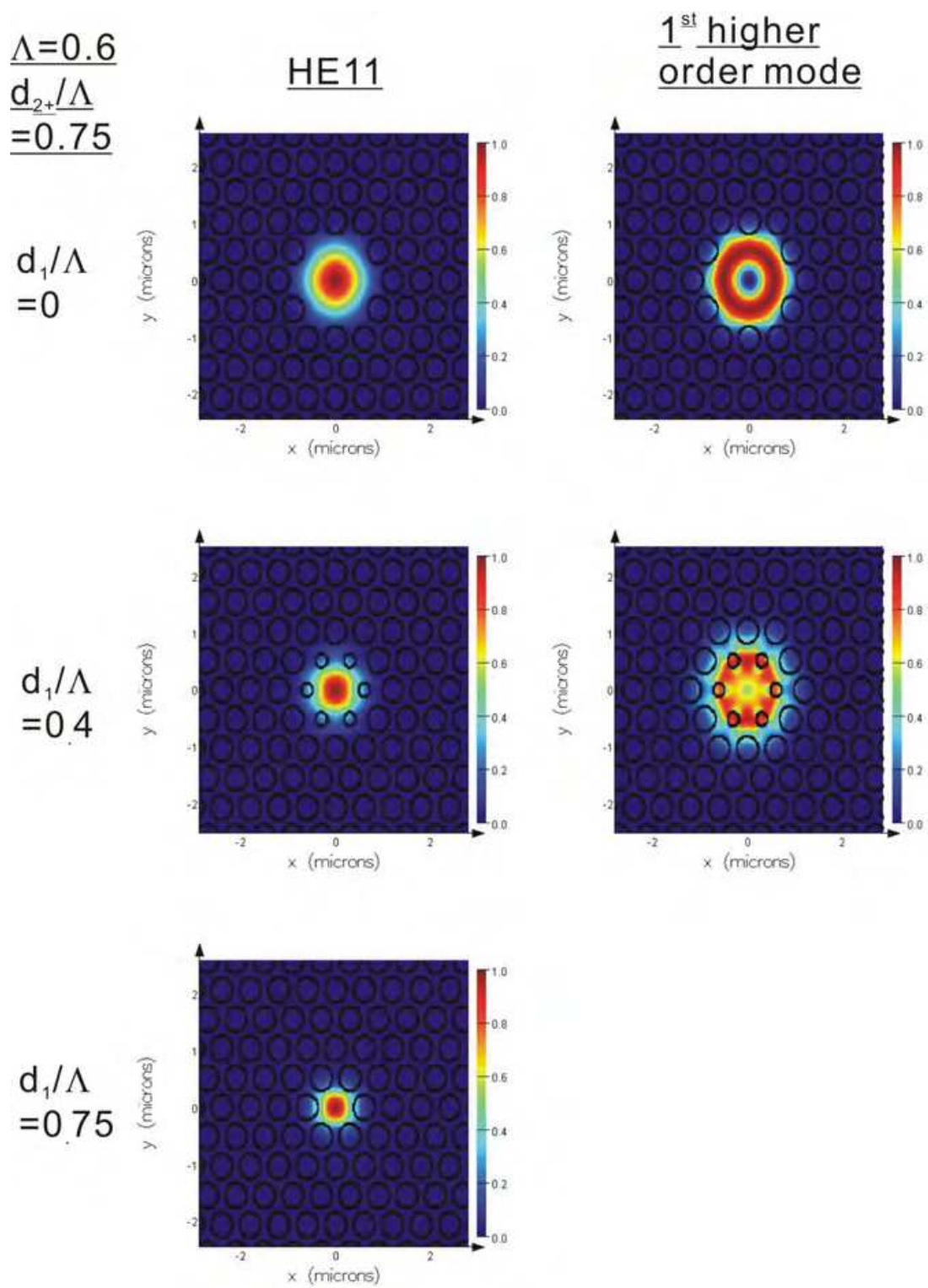d_{2+}/Λ
$=0.75$

HE11

$\underline{1^{st}\ higher}$
$\underline{order\ mode}$

d_1/Λ
$=0$

d_1/Λ
$=0.4$

d_1/Λ
$=0.75$

Fig. 4. Simulated modal field images of the HE11 mode and the 1st higher order mode for a taper design with $\Lambda=0.6$ μm and $d_{2+}/\Lambda= 0.75$, when $d_1/\Lambda= 0$, 0.4 and 0.75.

4.1 Dispersion

Dispersion profiles of the fundamental modes simulated from selected cross-sections along five MOF tapers are presented in Fig. 5. The MOF taper designs covered a large range of normal and anomalous dispersion at 1060 nm wavelength. Moreover, relatively flat dispersion slopes were found in many simulated cross-sections, especially at 1060 nm. The convex, flattened and decreasing dispersion profile would provide the ideal condition for generation of highly uniform and stable supercontinuum, which is required in telecommunications spectral slicing applications. Supercontinuum generated separately in MOFs with similar dispersion profiles pumping at 1060 nm had been studied experimentally (Tse et al., 2006a), but not in a single taper. If MOF taper technology is to be employed in optical communications networks, then the proposed constant fibre outer diameter is preferred when connecting to standard fibre via strong fusion splicing (Tse et al., 2009a; Chen et al., 2009b).

Fig. 5 shows that for various designed feature parameters, different dispersion profiles were found at different position along the tapers. In general, the dispersion curves varied with Λ and d_{2+}/Λ according to some predictable patterns. At around 1060 nm, as d_1/Λ decreases, the dispersion curve moves toward the normal dispersion regime. However, the flattest point of the curve may shift away from 1060 nm wavelength, as clearly shown in fig. 5(b). For Λ= 0.6 μm, as d_{2+}/Λ decreases, the dispersion also moves toward the normal dispersion regime for the same d_1/Λ, see for example, Fig. 5(b), (d) and (e), d_1/Λ= 0.2 and 0.3. Therefore, a greater portion (assuming constant rate of variation in d_1/Λ) of taper falls in the anomalous dispersion regime for a design with larger d_{2+}/Λ. It is less predictable for d_{2+}/Λ= 0.9 and varying Λ. The gradient of the curves varied asymmetrically in the wavelength range studied here. In practice, these results provide some valuable fabrication tolerance levels.

Individual dispersion profiles similar to or better than those shown in Fig. 5 can be achieved in fibres without longitudinal variation, however, to achieve multiple profiles in a single fibre, longitudinal variation is required (i.e. a fibre-taper).

For some applications, for example, soliton compression, a large anomalous dispersion variation may be preferred. However, if single-mode guidance is required, the dispersion profiles should be studied together with the confinement loss results presented in Fig. 3. In some cases, at the 7-cell core end, a few modes are supported in the core. For most applications, it is likely that only part of a MOF taper is useful, and not the entire length that d_1/Λ varied from 0 to d_{2+}/Λ. The unwanted portions can either be discarded, or shorten in length during the fibre drawing process.

4.2 Effective mode area

The effective mode area of the fundamental mode at 1060 nm pump wavelength is studied. As shown in Fig. 6, the effective area decreases along each MOF taper as the core-size decreases with d_1/Λ increases. For Λ= 0.5, 0.6 and 0.7 μm, part of the tapers has a sub-wavelength core size, thus greatly enhanced the nonlinearity. At the output of the tapers with d_{2+}/Λ= 0.9, the minimum effective area (A_{eff}) is around 0.65 μm², the nonlinearity (γ) is > 200 W⁻¹km⁻¹ at 1060 nm. For Λ= 0.7 μm, the end-to-end A_{eff} ratio is about 3, A_{eff}= 2.02 μm² at the input, however, a large portion of the taper is multi-mode. For Λ= 0.6 μm, smaller portion of the tapers is multi-mode, but at the expense of the A_{eff} ratio. For a MOF taper design with 8 rings of air holes, Λ= 0.6 μm and d_{2+}/Λ = 0.9, A_{eff}= 1.58 μm² at the input, the confinement loss of the entire taper is less than 0.0002 dB/m.
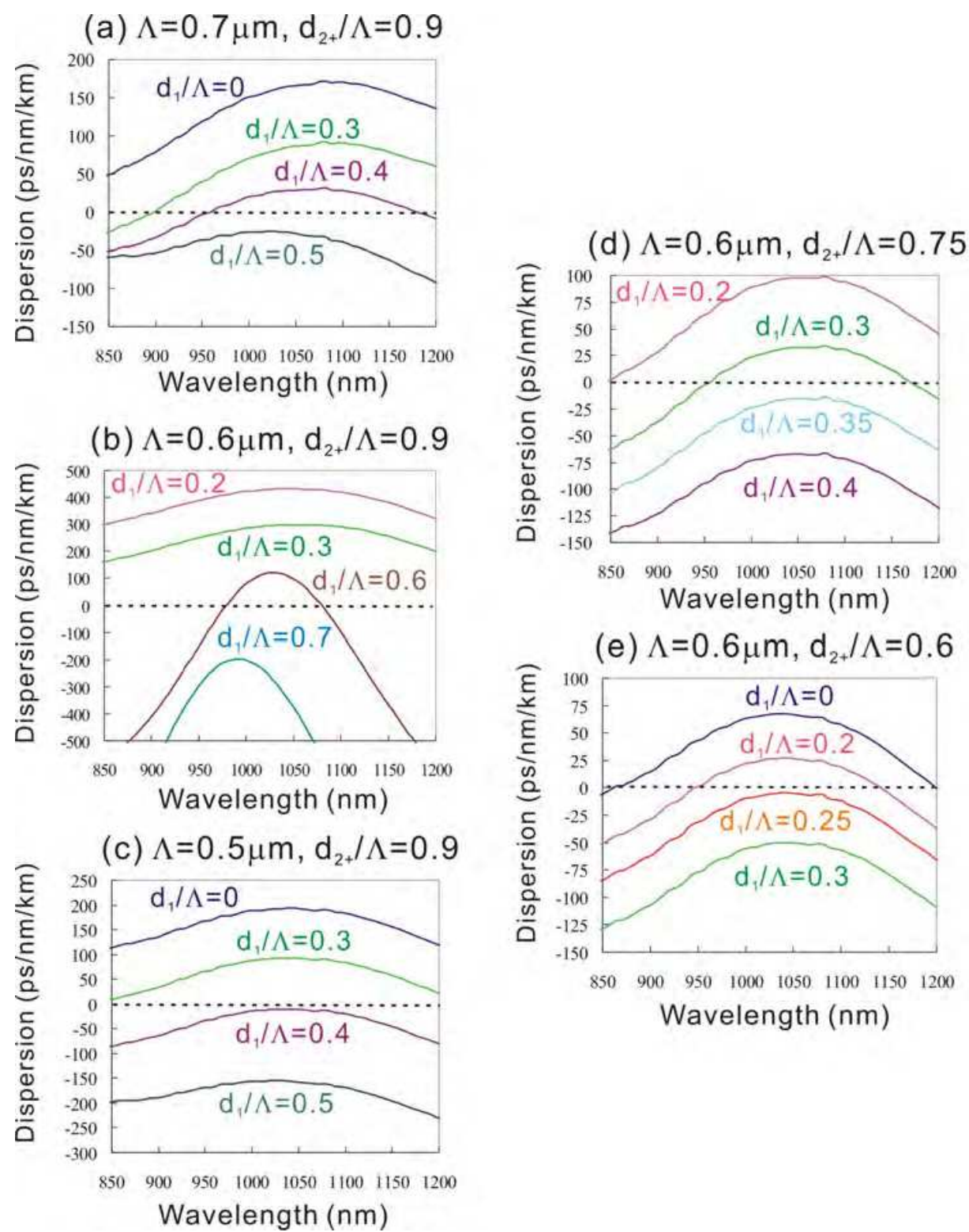
Fig. 5. Simulated dispersion profiles of the fundamental mode around 1060 nm at different position along five tapered fibres with different Λ and d_{2+}/Λ: (a) $\Lambda= 0.7$ µm and $d_{2+}/\Lambda= 0.9$, (b) $\Lambda= 0.6$ µm and $d_{2+}/\Lambda= 0.9$, (c) $\Lambda= 0.5$ µm and $d_{2+}/\Lambda= 0.9$, (d) $\Lambda= 0.6$ µm and $d_{2+}/\Lambda= 0.75$, (e) $\Lambda= 0.6$ µm and $d_{2+}/\Lambda= 0.6$.

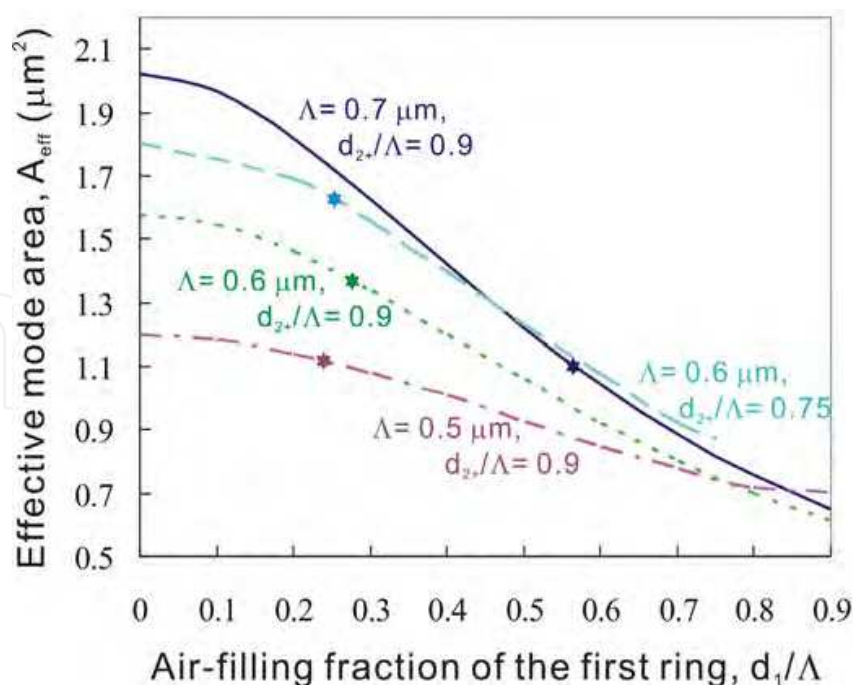Fig. 6. Simulated effective mode area profiles along 4 tapered fibres with different Λ and d_{2+}/Λ. (Asterisks indicate where CL of the 1st higher order mode is 10,000 times larger than that of the fundamental mode)

5. Fibre fabrication

In this section, a possible method for the fabrication of the proposed fibre-taper design is described by a modified capillaries stacking technique with multi-pressure hole-size control (Tse, 2007). The proposed generic method is given in Section 5.1 and the early fabrication result is presented in Section 5.2

5.1 Proposed fabrication method
Fig. 7 illustrates the modified capillary stacking method. The scheme consists of a traditional stack of open-ended and rigid capillaries in a holding tube, see Fig. 7(a). (Note that, the usual microstructured preform is made by stacking capillaries that are sealed at the top end.) Additional capillaries with smaller diameter are inserted into the open-ended capillaries. The outer diameter (perhaps 250 µm to 400 µm) of the inserted capillaries should be of good-fit to the inner diameter of the rigid capillaries. The flexible capillaries will provide the necessary physical elasticity for connecting to different pressure channels. Therefore, the pressure or hole-size of each hole can be controlled independently during fibre-draw. Here, we only need to consider controlling the pressure in each ring-of-holes. Since our design only require tapering one ring-of-holes (ring 1), and hole-size in rings 2 to 8 are to be kept constant, thus only two pressure regulatory channels are needed.

The modified stacking technique should work for both one-stage and two-stage fibre-draw. For one-stage draw, fibre is drawn directly from the stack. For 2-stage draw, the stack is drawn into cane first, an extra jacketing tube is added, then the jacket and cane are drawn together into fibre, see Fig. 7(b). The interstitial holes should collapse if the fibre is drawn close to 2000 ^{0}C with low draw-tension.

Rings 2-8 to
pressure
channel 2

Ring 1 to
pressure
channel 1

Flexible
capillaries

Holding tube

Packing rods

Core rod   Rigid
open-ended
capillaries

Jacketing tube
(if two-stage
draw is
required)

Cane (or
directly
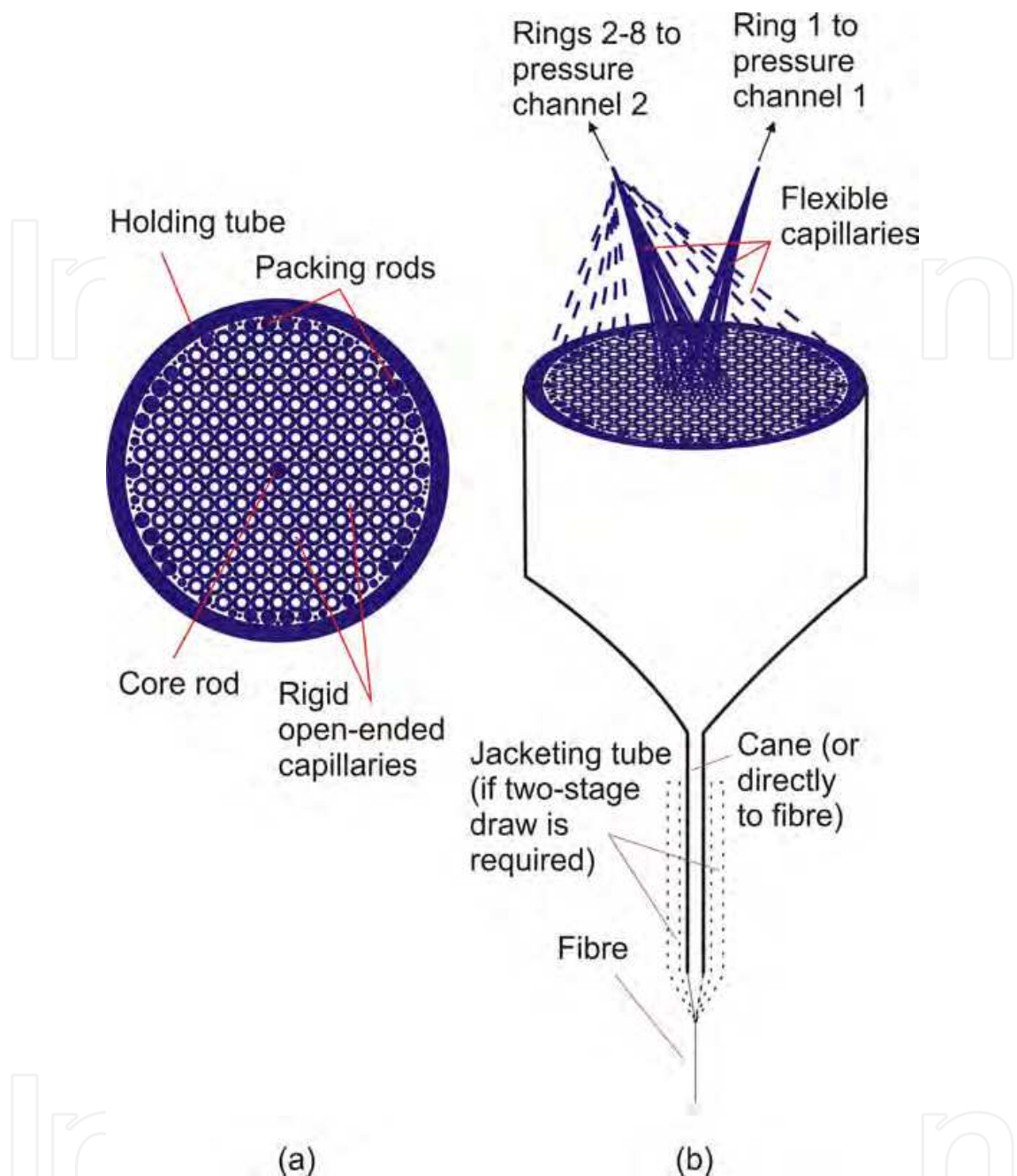to fibre)

Fibre

(a)   (b)

Fig. 7. A schematic of the proposed MOF taper fabrication method. (a) End-view of the stacking arrangement. (b) Shows the inserted flexible capillaries extension which can be connected to different pressure regulatory channels.

The main challenges will be on improving the pressure regulatory management system, the connection of the flexible capillaries to the pressure channels, and the feedback control of the fibre drawing system. In order to precisely control the hole-sizes, accurate active pressurisation is required. The pressures needed are often small, ranged to within a few millibars. Fibre draw tower should be equipped with fast and accurate pressure regulatory, drawing temperature and outer diameter feedback controls.

Constant pressure should be applied to all the holes when establishing the initial stable fibre drawing state. With all the feedback controls mentioned above, the pressure in the first ring-of-

holes can then be decreased gradually to form the required taper structure. In previous experiment (Tse et al., 2006b), collapsing of holes using the capillaries self-pressurise method during fibre-draw can be stable and smooth. Similar stable draw can be expected for the active pressurise method proposed here, see the next section for some preliminary results.

5.2 Active pressure fabrication experiment
5.2.1 One-stage cane drawing
In this section, the effect of active pressure made to a stacked preform is experimentally investigated. A relatively loose stack with only 2 ring-of-holes is used in this experiment. The whole perform is made of high grade low OH F300 silica glass. The stack arrangement and a photo of the preform are shown in Fig. 8. The preform is 1200 mm in length, consisted of 1 core rod with diameter of 1 mm, 20 rigid capillaries with outer diameter (OD) of 0.800 mm and inner diameter (ID) of 0.520 mm, 7 flexible capillaries with OD= 0.335 mm and ID= 0.220 mm, and a holding tube with OD= 12 mm and ID= 4.3 mm.

Holding tube:
OD=12mm
ID=4.3mm
L=1200mm

Core rod: 1000μm.
Inner ring: Open-ended capillaries with OD=800μm and ID=520μm.
            Flexible capillaries with OD=335μm and ID=220μm.
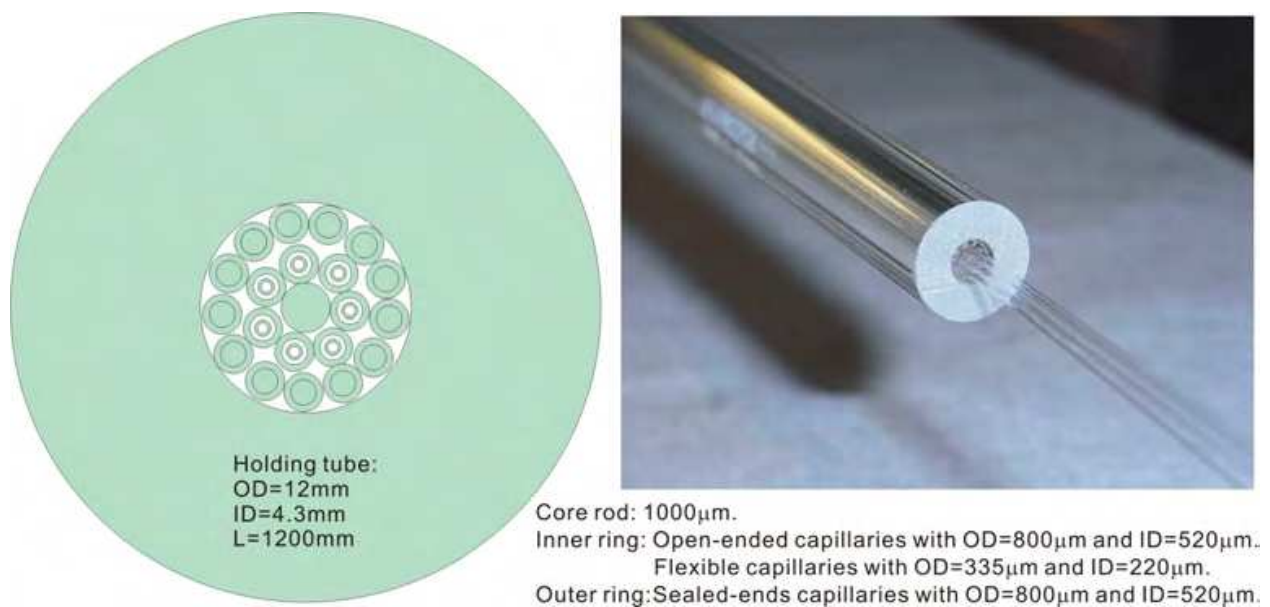Outer ring: Sealed-ends capillaries with OD=800μm and ID=520μm.

Fig. 8. (Left) A scaled schematic of the stack arrangement of the preform used in the active pressure experiment. (Right) A photo of the stacked preform with the flexible capillaries extended out. The dimensions of the stack elements are included in the figure.

The preform is arranged with the core rod surrounded by 7 open-ended capillaries, which forms the inner ring. A further 7 flexible capillaries are inserted in the inner ring, and extended out from the top of the rigid part of the preform. The flexible capillaries are then connected to a nitrogen pressure channel accordingly. The outer ring had 13 sealed-ends capillaries arranged closely around the wall of the holding tube. Therefore, active pressure is applied to the inner ring-of-holes only, and the outer ring is self-pressurised. According to the study carried out by Voyce et. al., the pressure inside a sealed capillary can remain relatively constant provided that long length is used and significantly extended out upward from the furnace, which is the case here (Voyce et. al., 2009). This setup will provide the necessary differential pressure for different ring-of-holes during draw to demonstrate the generic fabrication method proposed in section 5.1. The inner holes should stay open with a pressure

of >2.73 kPa, suggested in the work done by Wadsworth et. al. following a simple relationship of $P_{st}(kPa)= 600/d(\mu m)$, where Pst is the pressure required in unit of kilopascal to prevent a hole with diameter d in unit of micron from collapsing (Wadsworth et. al., 2005). The preform is drawn to cane size with OD of around 1.2 mm using a tractor belt puller. The drawing temperature was 1905 °C, the preform feeding speed was 10 mm/min, the pulling speed was 1 m/min, and the initial pressure applied to the inner ring was 8 kPa. At low temperature hole collapsing due to surface tension is reduced significantly. The furnace resistance graphite element has a diameter of >50 mm, with a capillary stack of ~4.3 mm wide loaded in the middle of the furnace, the temperature gradient across the stack is minimised. Note that, the preform is drawn without vacuum, which is often used in a traditional MOF drawing to get rid of the interstitial space and to help expanding the holes by introducing a negative pressure in the region. Thus the drawing conditions presented here led to a more accurate result of the effect caused to the capillaries by actively controlling the pressure in the holes only, with space for shrinkage and expansion.

The cane drawing result is summarised in Fig. 9, presented as microscope images of the cross-section. A total length of ~50 m of canes is drawn. Three pressure values were set during the draw, started at 8 kPa, then subsequently changed to 16 kPa → 11 kPa → 8 kPa → 11 kPa. The effect of the pressure change can be seen clearly from the pictures shown in Fig. 9 at different draw distance. By doubling the initial pressure of 8 kPa to 16 kPa, the pressure experienced by the holes was clearly over the set pressure of 16 kPa, see Fig. 9(a). This is because a lagging time is required for the pressure to stabilise by the pressure feedback loop control. It would be better to increase the pressure by small increment for a more stable hole-size increase. For the dimension of capillaries used in this preform, 16 kPa would inflate the inner holes and over power the outer ring-of-holes almost completely. At 11 kPa, the inner holes are almost at balance in pressure with similar size to the outer holes. At 8 kPa, shrinkage of the 7 inner holes relative to the outer holes is clearly visible. The outer holes were almost constant in size with pressure applied to the inner holes at 8 kPa and 11 kPa (Fig. 9(d)-(j)), which confirmed that a constant pressure is possible with long sealed-ends capillaries under self-pressurisation. It was found that decreasing pressure gave a more stable result without pressure over shooting the set point.

The study carried out in this section provide some useful data as a starting point for realising fibre-tapers on a fibre draw tower. It shows that an accurate control of selective hole-size is possible during one-stage cane-draw with active pressure. Optimal structure was achieved with a pressure of ~11 kPa, which is about 4x of the suggested pressure (P_{st}) required to prevent hole from collapsing.

5.2.2 Two-stage fibre drawing

The process of cane drawing studied in the previous section represents an one-stage draw with selective pressure control, and well controlled fibre structures were obtained. Next, a cane with the 7 inner holes connected to the same pressure control is inserted into a jacketing tube (OD= 12 mm, ID= 4.3 mm), and the outer holes were again subjected to self-pressurisation. The cane is being drawn to fibre as a two-stage draw with selective active pressure control.

The microscope image of the cane used in the fibre-draw is shown in Fig. 10(a), the diameter of the largest hole in the inner ring was assumed to be ~110 μm. The pressure applied to the inner holes was set initially at 5.5 kPa. The drawing temperature was 1905 °C, the preform
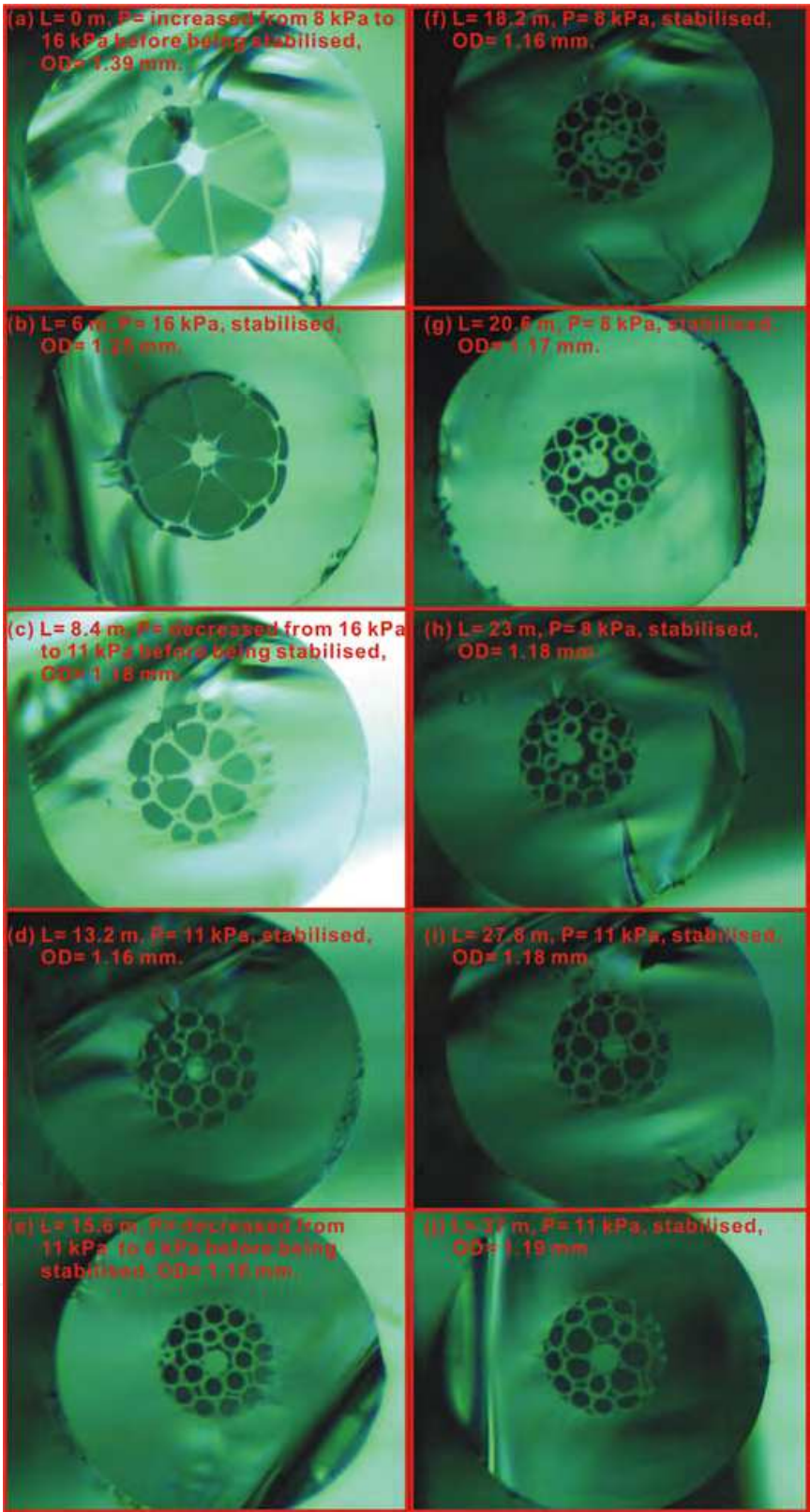
Fig. 9. Optical microscope images of the cross-section of the canes drawn from the preform with active pressure applied to the inner ring and self-pressurised for the outer ring. Draw temperature= 1905 °C, feed speed= 10 mm/min and draw speed= 1 m/min. The Draw length (L), active pressure (P) and outer diameter (OD) are included in the diagram.
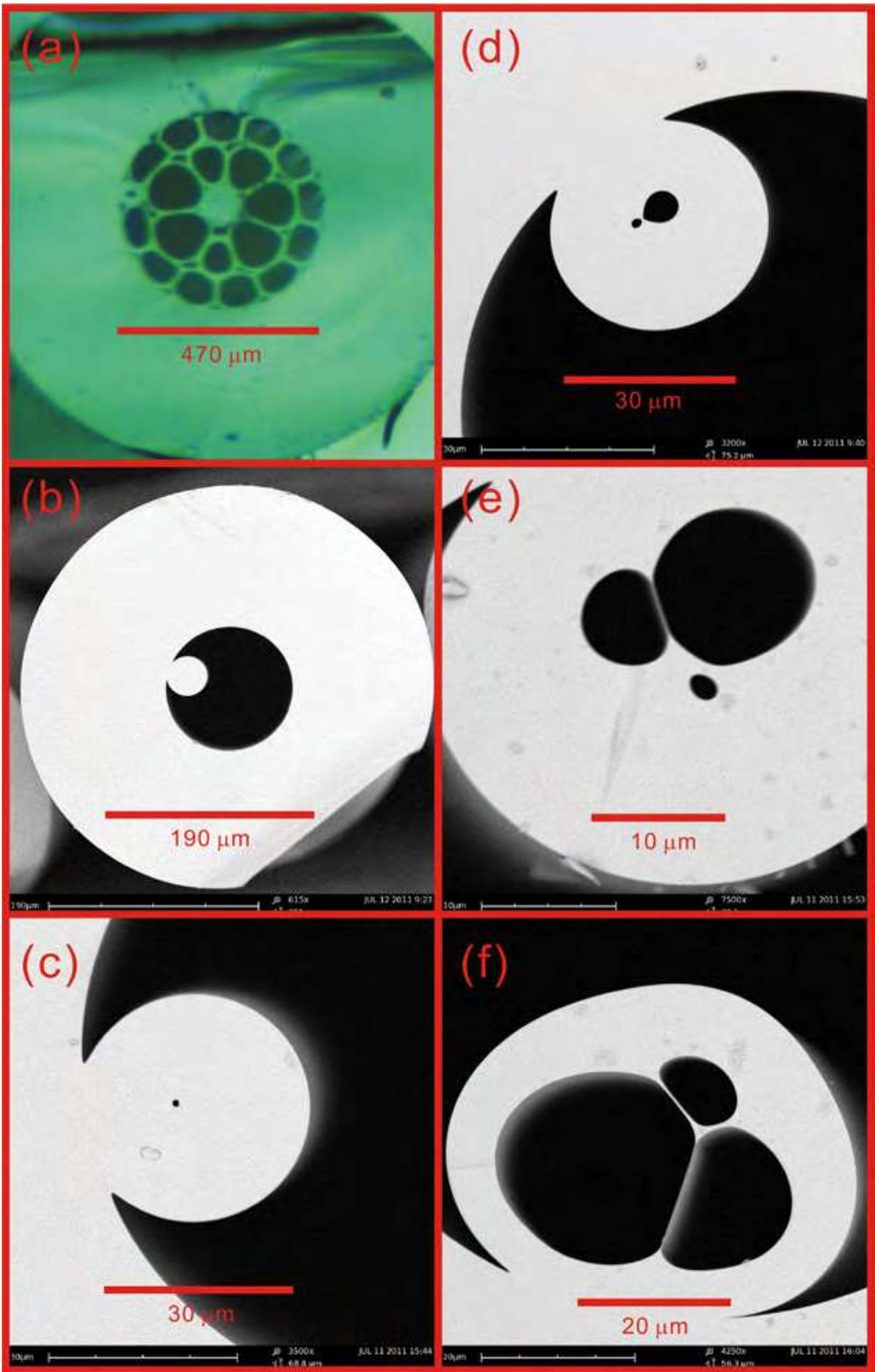
Fig. 10. (a) A photo to show the structure of the cane used in the two-stage fibre drawing experiment with active pressure control in the inner ring. (b) The SEM images of the fibre when pressure was below 18 kPa. (c)-(f) The SEM images of the fibre over the length of about 2 metres with pressure set point increased from 18 to 25.

feeding speed was 3 mm/min and the drawing speed was 3 m/min. No vacuum is applied to the space between the cane and the jacketing tube. The pressure in unit of kPa was then adjusted every few minutes to 5.8 → 6.2 → 6.7 → 7.3 → 8 → 9 → 11 → 14 → 18 → 25. The outer diameter of the fibre varied from 350 μm to 365 μm.

The SEM images of the fibre are shown in Fig. 10 (b)-(f). It was found that for pressure below 18 kPa, all the holes including the outer holes collapsed, with no structure found, SEM image of an example is presented in Fig. 10 (b). Some holes are opened and observed when the pressure was increased from 18 kPa to 25 kPa, see Fig. 10 (c)-(f). However, due to the large increment between the pressure set points, the pressure was increased too rapidly and was over shooting the set value, thus the holes in the cane massively expanded or 'burst' (picture excluded in the figure). A jacketing tube with ID closely fitted to the cane would solve the bursting problem.

Nonetheless, the effect of increasing pressure actively can be seen in a short portion of the fibre. The evolution of the fibre structure shown in Fig. 10 (c)-(f) only account for ~2 m of fibre in total. It is worth noting that not all 7 holes opened at the same time, and some may not open at all. This is because the hole-sizes of the 7 holes are different in the cane initially, and thus suggesting that it is a very important factor to consider when applying the same pressure to a ring-of-holes. The larger holes will open first and may dominate the structure. With the drawing conditions chosen, none of the outer holes opened under self-pressurisation, and only the largest holes are observed in the active pressured inner ring. Further study need to be carried out for pressure adjusted with small increment and for pressure decreases when the optimal pressure is known. The results obtained here suggest again, a pressure of ~$4P_{st}$ is prefer for obtaining good structure, and should be chosen to establish a stable draw initially.

Selective active pressure control method for MOF fabrication is demonstrated for both one-stage and two-stage fibre drawings. Further work need to be done by employing more than one pressure/vacuum channels, and refining the pressure adjustment, capillaries and jacketing tube selections in order to achieve the required fibre design.

6. Conclusions

A new design concept for microstructured fibre taper that can be produced on a traditional optical fibre draw tower with multi-pressure control is proposed. A study of the simplest case with different MOF parameters is presented. The design consists of the innermost ring-of-holes varied in size along the fibre, and outer rings with large holes of constant size to provide low confinement loss. The outer diameter of the taper is preserved with effective area taper ratio of between 2 and 3 is achieved. Potentially, larger ratio is possible by tapering more than one ring-of-holes, while the outer diameter for the taper is preserved. Designs with effective mode area as small as 0.65 μm² operating at 1.06 μm are simulated. Different designs offer different advantages depending on the application requirements. In general, this tapering concept offers low confinement, dispersion and nonlinearity tailoring, and high mechanical strength and ease of handling over the entire length of the MOF taper.

Early experiments demonstrated the feasibility for the proposed fabrication method with encouraging result. Further work is required to achieve the proposed fibre taper design.

The proposed active pressure control scheme not only produces tapered fibres, but other designs in three-dimensions. Preliminary experimental results showed that hole-size can be

selectively controlled longitudinally by both up-pressure and down-pressure; which suggest that fibre structure can be controlled comprehensively under general conditions. Similar scheme should also works for non-silica glass or polymer MOFs. By designing a more complex 2D fibre structure (Poletti et. al., 2005) together with the extra 3D design degree of freedom proposed here, one would expect this approach further extend the versatility of the microstructured fibre technology.

7. Acknowledgment

8. References

Baggett, J. C.; Monro, T. M.; Furusawa, K.; Finazzi V. & Richardson, D. J. (2003). Understanding bending losses in holey optical fibres, *Optics Communications*, Vol. 227, No. 4-6, (November 2003), pp. 317-335, ISSN 0030-4018

Bilodeau, F.; Hill, K. 0.; Faucher, S. & Johnson, D. C. (1988). Low-loss highly overcoupled fused couplers: fabrication and sensitivity to external pressure, *Journal of Lightwave Technology*, Vol. 6, No. 10, (October 1988), pp. 1476-1482, ISSN 0733-8724

Chen, Z.; Taylor, A. J. & Efimov, A. (2009a). Coherent mid-infrared broadband continuum generation in non-uniform ZBLAN fiber taper, *Optics Express*, Vol. 17, No. 7, (March 2009), pp. 5852-5860, ISSN 1094-4087

Chen, Z.; Xiong, C.; Xiao, L. M.; Wadsworth, W. J. & Birks, T. A. (2009b). More than threefold expansion of highly nonlinear photonic crystal fiber cores for low-loss fusion splicing, *Optics Letters*, Vol. 34, No. 14, (July 2009), pp. 2240-2242, ISSN 0146-9592

Chernikov, S. V.; Dianov, E. M.; Richardson, D. J. & Payne, D. N. (1993). Soliton pulse compression in dispersion-decreasing fibre, *Optics Letters*, Vol. 18, No. 7, (September 1993), pp. 476-478, ISSN 0146-9592

Couny, F.; Roberts, P. J.; Birks T. A. & Benabid, F. (2008). Square-lattice large-pitch hollow-core photonic crystal fibre, *Optics Express*, Vol. 16, No. 25, (November 2008), pp. 20626-20636, ISSN 1094-4087

Dudley J. & Coen, S. (2002). Numerical simulations and coherence properties of supercontinuum generation in photonic crystal and tapered optical fibres, *IEEE Journal of Selected Topics in Quantum Electronics*, Vol. 8, No.3, (May-June 2002), pp. 651-659, ISSN 1077-260X

Genty, G.; Coen S. & Dudley, J. M. (2007). Fibre supercontinuum sources, *Journal of the Optical Society of America B (Optical Physics)*, Vol. 24, No. 8, (August 2007), pp. 1771-1785, ISSN 0740-3224

Hu, J.; Marks, B. S.; Menyuk, C. R.; Kim, J.; Carruthers, T. F.; Wright, B. M.; Taunay, T. F. & Friebele, E. J. (2006). Pulse compression using a tapered microstructure optical fiber, *Optics Express*, Vol. 17, No. 9, (May 2006), pp. 4026-4036, ISSN 1094-4087

Nguyen, H. C.; Kuhlmey, B. T.; Steel, M. J.; Smith, C. L.; Mägi, E. C.; McPhedran, R. C. & Eggleton, B. J. (2005). Leakage of the fundamental mode in photonic crystal fibre tapers, *Optics Letters*, Vol. 30, No. 10, (May 2005), pp. 1123-1125, ISSN 0146-9592

Poletti, F.; Finazzi, V.; Monro, T. M.; Broderick, N. G. R.; Tse, V. & Richardson, D. J. (2005). Inverse design and fabrication tolerances of ultra-flattened dispersion holey fibers, *Optics Express*, Vol. 13, No. 10, (May 2005), pp. 3728-3736, ISSN 1094-4087

Town G. E. & Lizier J. T. (2001). Tapered holey fibers for spot-size and numerical-aperture conversion, *Optics Letters*, Vol. 26, No. 14, (July 2001), pp. 1042-1044, ISSN 0146-9592

Travers, J. C.; Stone, J. M.; Rulkov, A. B.; Cumberland, B. A.; George, A. K.; Popov, S. V.; Knight, J. C. & Taylor, J. R. (2007). Optical pulse compression in dispersion decreasing photonic crystal fibre, *Optics Express*, Vol. 15, No. 20, (October 2007), pp. 13203-13211, ISSN 1094-4087

Tse, M. L. V.; Horak, P.; Poletti, F.; Broderick, N. G. R.; Price, J. H. V.; Hayes, J. R. & Richardson, D. J. (2006a). Supercontinuum generation at 1.06 μm in holey fibres with dispersion flattened profiles, *Optics Express*, Vol. 14, No. 10, (May 2006), pp. 4445-4451, ISSN 1094-4087

Tse, M. L. V.; Horak, P.; Price, J. H. V.; Poletti, F.; He, F. & Richardson, D. J. (2006b). Pulse compression at 1.06 μm in dispersion-decreasing holey fibres, *Optics Letters*, Vol. 31, No. 23, (December 2006), pp. 3504-3506, ISSN 0146-9592

Tse, M. L. V. (2007). *Development and applications of dispersion controlled high nonlinearity microstructured fibres*, PhD thesis, University of Southampton, Southampton, U.K.

Tse, M. L. V.; Horak, P.; Poletti, F. & Richardson, D. J. (2008). Designing tapered holey fibres for soliton compression, *IEEE Journal of Quantum Electronics*, Vol. 44, No. 2, (February 2008), pp. 192-198, ISSN 0018-9197

Tse, M. L. V.; Tam, H. Y.; Fu, L. B.; Thomas, B. K.; Dong, L.; Lu, C. & Wai, P. K. A. (2009a). Fusion splicing holey fibres and single-mode fibres: a simple method to reduce loss and increase strength, *IEEE Photonics Technology Letters*, Vol. 21, No. 3, (February 2009), pp. 164-166, ISSN 1041-1135

Tse, M. L. V.; Tam, H. Y.; Lu, C. & Wai, P. K. A. (2009b). Novel design of a microstructured fibre taper, *Proceedings of 14th OptoElectronics and Communications Conference (OECC)*, ThLP32 , ISSN 978-1-4244-4102-0, Hong Kong, China, July 13-17, 2009

Voyce, C. J.; Fitt, A. D.; Hayes, J. R. & Monro, T. M. (2009). Mathematical modeling of the self-pressurising mechanism for microstructured fiber drawing, *Journal of Lightwave Technology*, Vol. 27, No. 7, (April 2009), pp. 871-878, ISSN 0733-8724

Vukovic, N.; Broderick, N. G. R.; Petrovich M. & Brambilla G. (2008). Novel method for the fabrication of long optical fibre tapers, *IEEE Photonics Technology Letters*, Vol. 20, No. 14, (July 2008), pp. 1264-1266, ISSN 1041-1135

Wadsworth, W. J.; Witkowska, A.; Leon-Saval, S. G. & Birks, T. A. (2005). Hole inflation and tapering of stock photonic crystal fibres, *Optics Express*, Vol. 13, No. 18, (September 2005), pp. 1094-4087, ISSN 1094-4087

White, T. P.; McPhedran, R. C.; Martijn de Sterke, C.; Litchinitser, N. M. & Eggleton, B. J. (2002). Resonance and scattering in microstructured optical fibres, *Optics Letters*, Vol. 27, No. 22, (November 2002), pp. 1977-1979, ISSN 0146-9592
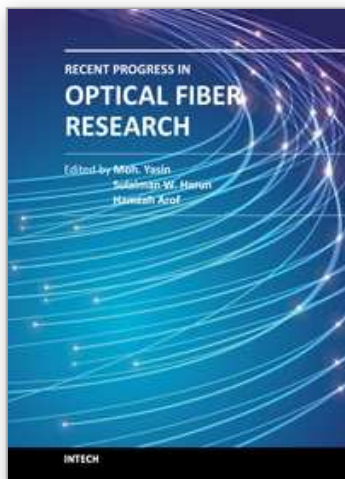
Recent Progress in Optical Fiber Research

Edited by Dr Moh. Yasin

This book presents a comprehensive account of the recent progress in optical fiber research. It consists of four sections with 20 chapters covering the topics of nonlinear and polarisation effects in optical fibers, photonic crystal fibers and new applications for optical fibers. Section 1 reviews nonlinear effects in optical fibers in terms of theoretical analysis, experiments and applications. Section 2 presents polarization mode dispersion, chromatic dispersion and polarization dependent losses in optical fibers, fiber birefringence effects and spun fibers. Section 3 and 4 cover the topics of photonic crystal fibers and a new trend of optical fiber applications. Edited by three scientists with wide knowledge and experience in the field of fiber optics and photonics, the book brings together leading academics and practitioners in a comprehensive and incisive treatment of the subject. This is an essential point of reference for researchers working and teaching in optical fiber technologies, and for industrial users who need to be aware of current developments in optical fiber research areas.

How to reference

In order to correctly reference this scholarly work, feel free to copy and paste the following:

Ming-Leung Vincent Tse, D. Chen, C. Lu, P. K. A. Wai and H. Y. Tam (2012). Microstructured Fibre Taper with Constant Outer Diameter, Recent Progress in Optical Fiber Research, Dr Moh. Yasin (Ed.), ISBN: 978-953-307-823-6, InTech, Available from: http://www.intechopen.com/books/recent-progress-in-optical-fiber-research/microstructured-fibre-taper-with-constant-outer-diameter

INTECH
open science | open minds